

Structure and gas sensitivity of $\text{WO}_3\text{-In}_2\text{O}_3$ and $\text{WO}_3\text{-Co}_3\text{O}_4$ oxide compositions

Yulyan S. Haiduk¹, Alexander A. Khort², Maxim A. Makhavikou¹, Alexander A. Savitsky¹

¹ Belarusian State University, 4 Nezavisimosti Ave., Minsk 220030, Belarus

² KTH, Royal Institute of Technology, Drottning Kristinas vag 51, SE-100 44 Stockholm, Sweden

Corresponding author: Yulyan S. Haiduk (j_hajduk@bk.ru)

Received 25 March 2019 ♦ Accepted 17 August 2019 ♦ Published 12 September 2019

Citation: Haiduk YuS, Khort AA, Makhavikou MA, Savitsky AA (2019) Structure and gas sensitivity of $\text{WO}_3\text{-In}_2\text{O}_3$ and $\text{WO}_3\text{-Co}_3\text{O}_4$ oxide compositions. *Modern Electronic Materials* 5(3): 115–125. <https://doi.org/10.3897/j.moem.5.3.52308>

Abstract

Using oxide compositions is a promising method of increasing the sensitivity and selectivity of semiconductor gas sensors on the basis of SnO_2 , In_2O_3 , WO_3 and other oxides. We have studied nanocrystalline tungsten oxide (WO_3), indium oxide (In_2O_3), cobalt oxide (Co_3O_4) and mixed oxide compositions with different $\text{WO}_3/\text{In}_2\text{O}_3$ and $\text{WO}_3/\text{Co}_3\text{O}_4$ ratios synthesized using the sol-gel method after xerogel annealing at 400–600 °C. The morphology, phase composition and structure of the materials have been studied using X-ray diffraction, infrared spectroscopy, scanning electron microscopy and transmission electron microscopy. We showed that stable structures can be produced in $\text{WO}_3\text{-In}_2\text{O}_3$ and $\text{WO}_3\text{-Co}_3\text{O}_4$ nanoheterogeneous compositions. The growth of grain size in WO_3 and In_2O_3 , WO_3 and Co_3O_4 during heat treatment of mixed compositions occurs slower than in simple oxides. An increase in the gas sensitivity of the compositions in comparison with simple oxides can be accounted for by smaller grain sizes and hence larger specific surface area, as well as by the dependence of grain surface state on material composition. Both compositions exhibit the greatest nitrogen dioxide response at 130–150 °C and the greatest carbon oxide response at above 230 °C. We have produced low-power nitrogen dioxide sensors with a sensitivity of $\ll 1$ ppm and power consumption of ≤ 85 mW.

Keywords

tungsten oxide, indium oxide, cobalt oxide, semiconductor gas sensor

1. Introduction

Using oxide compositions is a promising method of increasing the sensitivity and selectivity of semiconductor gas sensors on the basis of SnO_2 , In_2O_3 , WO_3 and other oxides [1]. Earlier [2–5] the structure and morphology of $\text{WO}_3\text{-In}_2\text{O}_3$ and $\text{WO}_3\text{-Co}_3\text{O}_4$ oxide compositions synthesized using the sol-gel method were studied. Xerogel annealing at 400 and 600 °C for 2 h in the $\text{WO}_3\text{-In}_2\text{O}_3$ system led to the formation of a heterogeneous two-phase material consisting of a monoclinic WO_3 phase and a cubic In_2O_3 phase. Annealing at 800–850 °C led to the

synthesis of $\text{In}_2(\text{WO}_4)_3$ [2]. Annealing at 400 °C for 2 h in the $\text{WO}_3\text{-Co}_3\text{O}_4$ system led to the formation of a heterogeneous two-phase material consisting of a monoclinic WO_3 phase and a cubic Co_3O_4 phase and annealing at 600–650 °C led to the synthesis of CoWO_4 [3]. The studies were carried out using thermogravimetry, differential thermal analysis, infrared spectroscopy, X-ray phase analysis and low-temperature nitrogen adsorption. The gas sensitivity of the $\text{WO}_3\text{-In}_2\text{O}_3$ and $\text{WO}_3\text{-Ga}_2\text{O}_3$ compositions to reducing (CO) and oxidizing (NO_2) gases increased due to strong structural disordering and grain size reduction in the compositions in comparison

with source simple oxides and an increase in the specific surface area of the material. Experiments showed that the $\text{In}_2(\text{WO}_4)_3$ and CoWO_4 compounds do not exhibit strong gas adsorption [3, 4].

Below we analyze experimental data on the structure and morphology of the abovementioned compositions annealed at 200–600 °C and the CO and NO_2 sensitivity of the specimens as a function of composition and temperature.

2. Experimental

Tungsten oxide WO_3 was obtained from a 1.23M water solution of $\text{Na}_2\text{WO}_3 \cdot 2\text{H}_2\text{O}$ by drop-by-drop addition to a 12M nitric acid solution with permanent stirring and the residual electrolyte was removed by decanting. Indium oxide In_2O_3 was obtained from a 0.78M water solution of $\text{In}(\text{NO}_3)_3 \cdot 4.5\text{H}_2\text{O}$ by adding 0.24M ammonia water solution. Similarly, cobalt oxide Co_3O_4 was obtained from a 2.3M water solution of $\text{CoSO}_4 \cdot 7\text{H}_2\text{O}$ by adding 0.24M ammonia water solution.

For physicochemical analysis the specimens were dried prepared sols at room temperature, mixing of xerogels in different weight ratios and heat treatment of the resultant compositions at 200–600 °C for 2 h in air. The electrical resistivity of the specimens was measured during heating and cooling with a B7-40 digital multimeter and the temperature was controlled with an aluminum thermocouple located near the specimen.

X-raying was carried out on a DRON-3 diffractometer in CoK_α radiation. The size of coherent scattering regions, i.e., the grain size in polycrystalline specimens, was determined from diffraction peak broadening (the Scherrer method) using the formula

$$D = \frac{0.9\lambda}{b \cos\theta} \quad (1)$$

where λ is the monochromatic X-ray wavelength, b is the peak width at half height and θ is the diffraction angle [6].

The infrared spectra of the specimens dried at 20, 300 and 600 °C were taken with an AVATAR 330 (Thermo Nicolet) spectrometer at wavenumbers $\nu = 400\text{--}700 \text{ cm}^{-1}$. The diffuse scattering spectra were recorded with a Smart Diffuse Reflectance unit. Xerogel powders dried at 20 °C were examined on a Netzsch STA 449C Jupiter synchronous thermal analysis instrument at 20–600 °C in the air at a 5 K/min heating rate. The charge weight was 2.47–2.92 mg.

The microstructure of the specimens was examined under a LEO 1420 scanning electron microscope.

Transmission electron microscope (TEM) was used for studying the size and structural morphology of compositions under a Hitachi H-800 microscope at 200 keV acceleration voltage. Before TEM examination and electron diffraction pattern taking the specimens were annealed at a preset temperature and dispersed by ultrasonication in water. The suspension was applied onto a polyvinyl-formal mesh.

The specific surface area of the powders was determined from low-temperature nitrogen adsorption on a Klyatchko–Gurvich instrument [7].

The specimens were prepared in the form of pellets 10.0 mm in diameter and 3.0 mm in thickness weighing 0.7–0.8 g pressed from preliminarily annealed powdered oxides (400 °C, 2 h) with an organic binder (colophony) under a hydraulic press at a 150 kPa pressure and sintered at 450 °C for 5 h in air. Silver electrodes were applied at both sides of the specimens for improving the quality of the electric contact. Two-electrode sensors were produced by depositing WO_3 and $\text{WO}_3\text{-Co}_3\text{O}_4$ compositions onto $1.3 \times 1.3 \text{ mm}^2$ anodized aluminum microplates with platinum electrodes by photolithography followed by annealing at 450 °C for 12 h in air.

The sensor response S (rel. units) was determined using the formula

$$S = R_a/R_{\text{og}},$$

where R_a and R_{og} are the electrical resistances of the pellet (the sensor) in air and NO_2 oxidizing gas, respectively, or using the formula

$$S = R_{\text{ig}}/R_a,$$

where R_a and R_{ig} are the electrical resistances in air and CO reducing gas, respectively. The gas sensitivity of the compositions was studied using carbon oxide containing test gas mixtures produced by Minsk Research Institute for Radio Engineering Materials. The gas mixtures for nitrogen dioxide sensitivity study of the compositions in the form of gas permeable pellets were prepared as described earlier [8].

3. Results and discussion

Xerogel of hydrated tungstic acid $\text{H}_2\text{WO}_4 \cdot \text{H}_2\text{O}$ (PDF 87-2404) was obtained from sodium tungstate. Then the xerogel lost water during annealing and crystallized in the form of a monoclinic WO_3 modification (PDF 43-1035). Annealing of tungstic acid xerogel at 300–900 °C for 2 h in the air led to the formation of tungsten oxide. The size of coherent scattering regions increased with annealing temperature from 70 nm at 200 °C to 100 nm at 600 °C. The lattice parameters of the WO_3 monoclinic structure were found almost constant during annealing at 200–800 °C and equal to $a = 7.299\text{--}7.328 \text{ nm}$, $b = 7.527\text{--}7.537 \text{ nm}$, $c = 7.698\text{--}7.732 \text{ nm}$ and $\beta = 90.90\text{--}91.40 \text{ arc deg}$.

Xerogel obtained from indium nitrate after drying at 20 °C is amorphous $\text{In}(\text{OH})_3$. Comparison of X-ray powder diffraction patterns after $\text{In}(\text{OH})_3$ annealing at 200–800 °C showed that In_2O_3 is the predominant phase after annealing at 200 °C for 2 h. Its sintering leads to an increase in the coherent scattering region size from 10–12 nm after annealing at 200 °C, to 20 nm after annealing at 300 °C, 35 nm after annealing at 600 °C and 50 nm

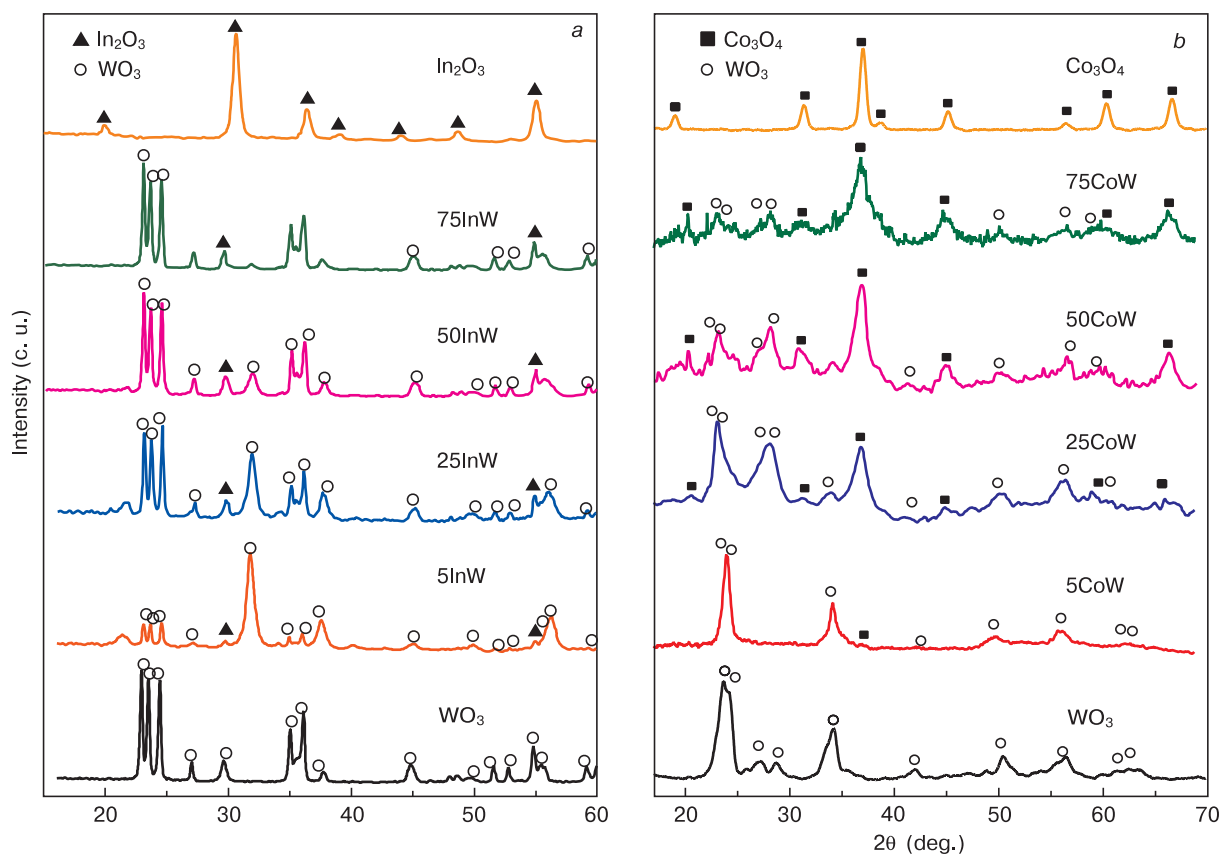


Figure 1. Spectra of X-ray phase analysis of samples of oxides of tungsten, indium and cobalt, as well as their compositions, obtained under various conditions of annealing: (a) 600 °C, 2 h, (b) 400 °C, 2 h.

after annealing at 850 °C. The lattice parameter a of In_2O_3 did not change after annealing at 200–800 °C, remaining 1.008–1.015 nm.

Cobalt sulfate xerogel consisted of a mixture of $\text{Co}(\text{OH})_2$ (PDF 45-31) and $\text{Co}(\text{OH})_2$ (PDF 2-925). These compositions decomposed at 200–800 °C to form Co_3O_4 in a cubic structure. The coherent scattering region size of the Co_3O_4 specimen was 80 nm after annealing at 200 °C, 160 nm after annealing at 400 °C and 250 nm after annealing at 600 °C. The lattice parameter a of Co_3O_4 did not change after annealing at 200–800 °C, remaining 0.8064–0.8084 nm.

X-ray phase analysis showed that the WO_3 – In_2O_3 (20 °C) and WO_3 – Co_3O_4 (20 °C) xerogel powders containing 5.0, 25.0, 50.0 and 75.0 wt.% of In_2O_3 or Co_3O_4 were amorphous. Annealing at 200–450 °C for 2 h did not change the two-phase composition of the WO_3 – Co_3O_4 , and annealing at 600 °C led to the formation of a third by-phase CoWO_4 . Annealing of the WO_3 – In_2O_3 samples (5InW, 25InW, 50InW and 75InW) at 600 °C led to the formation of a heterogeneous two-phase composition with a coherent scattering region size of ~30–35 nm. Annealing of the WO_3 – Co_3O_4 samples (5CoW, 25CoW, 50CoW and 75CoW) at 400 °C led to the formation of a heterogeneous two-phase composition with a coherent scattering region

size of ~50 nm. Figure 1 shows X-ray diffraction patterns of the WO_3 , In_2O_3 and Co_3O_4 samples and the test compositions 5InW, 25InW and 75InW, annealed at 600 °C, and 5CoW, 25CoW and 75CoW, annealed at 400 °C.

Annealing of the WO_3 – In_2O_3 system at 800–850 °C for 2 h triggered a solid-state reaction producing a heterogeneous material the main phase of which was $\text{In}_2(\text{WO}_4)_3$ (PDF 49-0337). The WO_3 – In_2O_3 specimens for gas adsorption tests were annealed at 450 and 650 °C. It was founded, the $\text{In}_2(\text{WO}_4)_3$ phase did not form upon annealing. The coherent scattering region sizes of WO_3 in the WO_3 – In_2O_3 specimen containing 25.0 wt.% In_2O_3 after annealing at 400 and 500 °C for 2 h were ~25 and ~35 nm, respectively, which is significantly smaller than those of the WO_3 powders (~100 and ~110 nm, respectively) annealed under the same conditions.

The X-ray diffraction patterns of the specimens annealed at 400 °C did not contain CoWO_4 peaks (Fig. 1b). The size of coherent scattering region of the 25CoW specimen is ~50 nm which is also smaller than for simple tungsten oxide specimens (~100 nm) and cobalt oxide specimens (~200 nm) annealed under the same conditions. This can be caused by the formation of grains with distorted uneven faces impeding their growth in complex oxide systems with different crystalline structures [10].

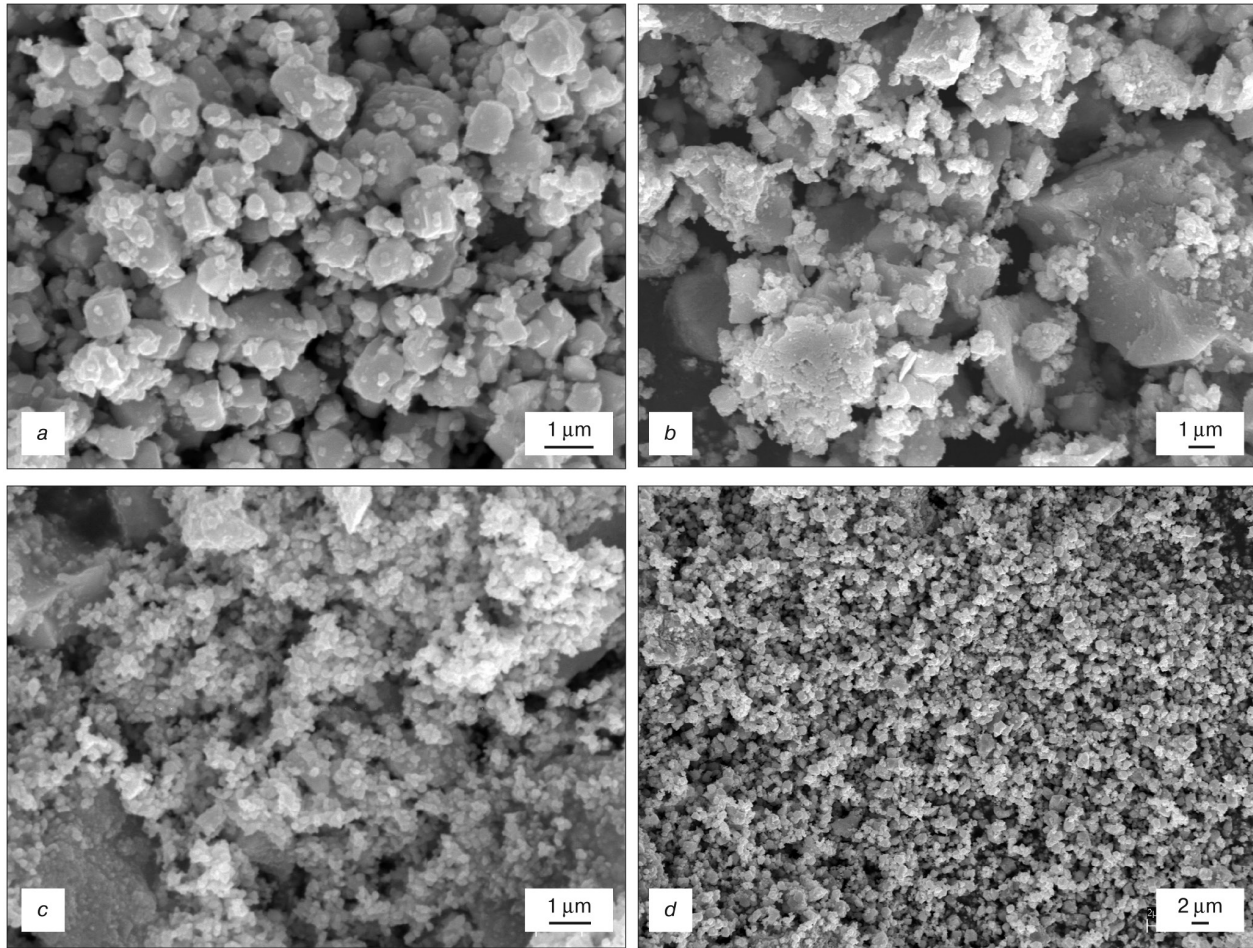


Figure 2. Micrographs of the surface of oxide materials obtained by scanning electron microscopy: (a) WO_3 , (b) In_2O_3 , (c) 25InW, (d) 15CoW.

Thus joint annealing of tungstic acid and indium or cobalt hydroxide xerogels suppresses grain growth in comparison with simple oxides. A decrease in coherent scattering region size usually increases the gas sensitivity of gas sensors and lowers their operation temperature [1].

Figure 2 shows scanning electron microscopy (SEM) images of (a) WO_3 , (b) In_2O_3 , (c) 25InW and (d) 15CoW mixed compositions. The WO_3 powder (Fig. 2a) is a mixture of homogeneous spherical particles locally forming agglomerations on the surfaces of which the boundaries of individual particles could be well resolved. The amount of particles with sizes less than 250 nm is 706 per 1000 particles with a surface distribution density of $\approx 3.3 \mu\text{m}^2$. Within the fraction of particles sized 0–250 nm one can easily resolve irregularly shaped particles 50+ nm in diameter. Large particles (up to 2.5 μm) are agglomerations of planar plates with smooth or sharp edges. One can clearly see the step-like structure of the agglomerations formed by single thin plates. The shapes and sizes of WO_3 particles are similar to those described in the literature [10–14].

In_2O_3 powder (Fig. 2b) is a mixture of particles with different shapes and sizes. The fraction of particles sized less than 250 nm is 348 per 1000 particles, with the surface distribution density of $\approx 3.06 \mu\text{m}^2$. Within the frac-

Table 1. The specific surface area of the studied samples.

Sample	Heat treatment conditions	S, m^2/g
$\text{WO}_3 \times 2\text{H}_2\text{O}$	20 °C	32.0
WO_3	200 °C, 2 h	51.5
WO_3	400 °C, 2 h	24.0
WO_3	600 °C, 2 h	3.2
5InW	400 °C, 2 h	45.5
15InW	400 °C, 2 h	12.5
50InW	400 °C, 2 h	9.5
Co_3O_4	400 °C, 2 h	17.8
5CoW	400 °C, 2 h	40.5
15CoW	400 °C, 2 h	19.5

tion of particles sized 0–250 nm one can easily resolve irregularly shaped particles 50+ nm in diameter. Unlike WO_3 and Co_3O_4 , In_2O_3 powder has a smaller particle size scatter and a larger fraction of bigger particles.

SEM image of the 25InW sample (Fig. 2c) shows that the powdered mixture of irregularly shaped nanosized particles (50–150 nm) consists of relatively homogeneous grains sometimes forming agglomerations. The fraction of particles with a size of less than 250 nm is 925.72 per 1000 particles with a surface distribution density of $\approx 25.21 \mu\text{m}^2$. Within the fraction of particles sized 0–250 nm one can easily resolve irregularly shaped par-

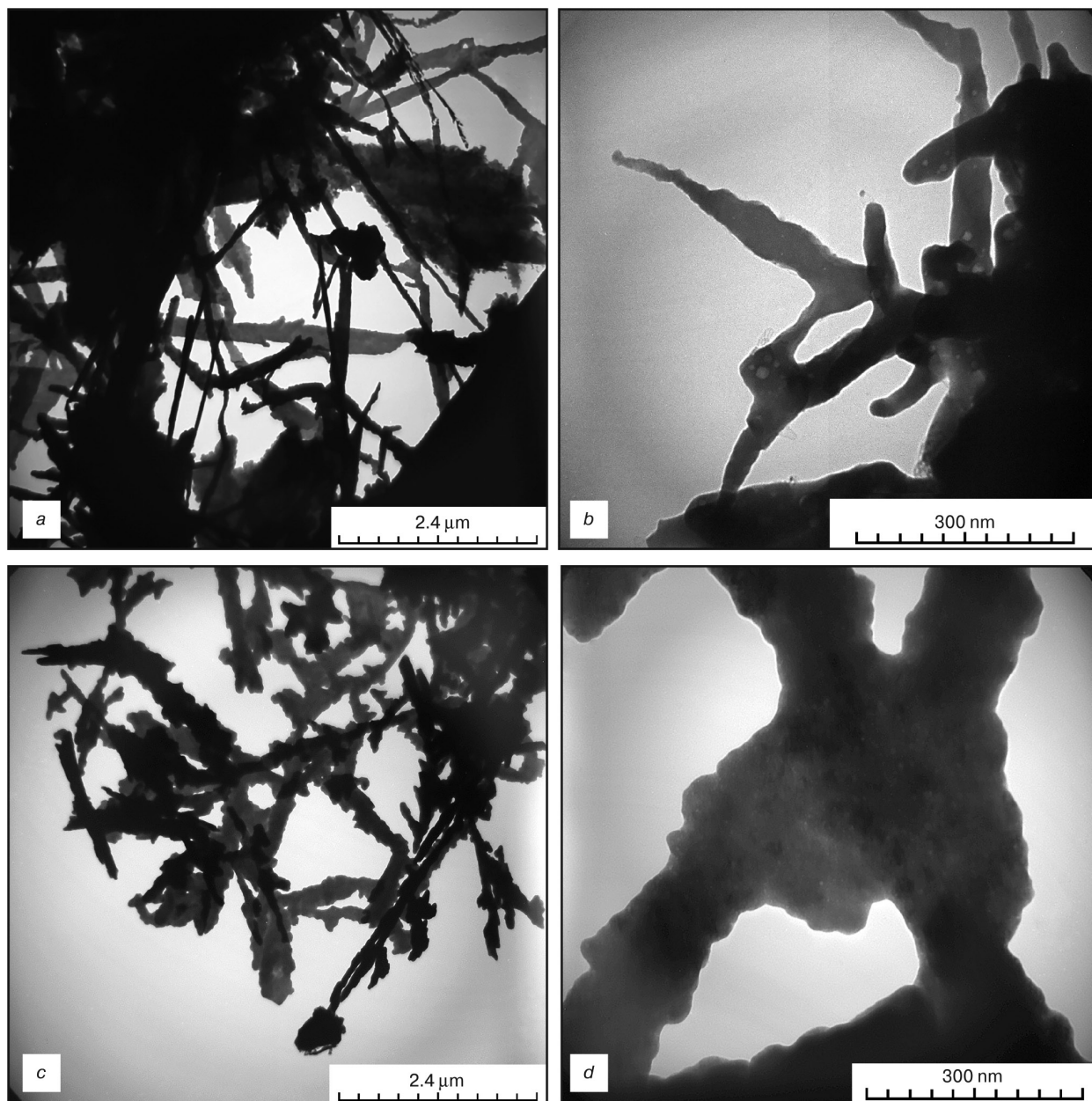


Figure 3. TEM images of powders (*a, b*) 25InW and (*c, d*) 25CoW.

ticles 50+ nm in diameter. Large individual particles (to 2.0 μm) are agglomerations of planar plates. The fraction of particles sized less than 500 nm is 982.63 per 1000 particles with the surface distribution density of $\approx 10.67 \mu\text{m}^2$.

The 15CoW powder (Fig. 2*d*) contains significantly smaller particles and has a high value of specific surface area (0.2–0.3 μm and 12.4 m^2/g for 15CoW and 0.2–2 μm and 3.2 m^2/g for WO_3 , respectively). Thus, according to SEM analysis, the sizes of the WO_3 , In_2O_3 and Co_3O_4 particles after heat treatment of mixed compositions are less than the size of simple oxide powders.

Analysis of the SEM images showed a decrease in the particle sizes in the compositions which agrees with the greater specific surface area of mixed compositions in comparison with simple oxide powders (Table 1).

Figure 3 shows TEM images of 25InW and 25CoW powders. The TEM micrographs clearly resolve individual phases of heterogeneous compositions where the grey contrast regions refer to the In_2O_3 (Fig. 3*a, b*) and Co_3O_4 (Fig. 3*c, d*) phases and dark contrast regions are the WO_3 phase (Fig. 3*a–d*). The particles are needle-shaped and have a size from 0.32 to 3 μm . We believe this particle shape determines a large specific surface area of the materials.

IR spectra of WO_3 , In_2O_3 and Co_3O_4 powders heat-treated at 200–600 $^\circ\text{C}$ were obtained and analyzed earlier [2, 3, 5]. For higher annealing temperatures the band of W–O valence oscillations (500–900 cm^{-1}) is more intense and better resolved due to WO_3 dehydration. The strong absorption band in the 450–900 cm^{-1} region is commonly attributed to W–O oscillations in

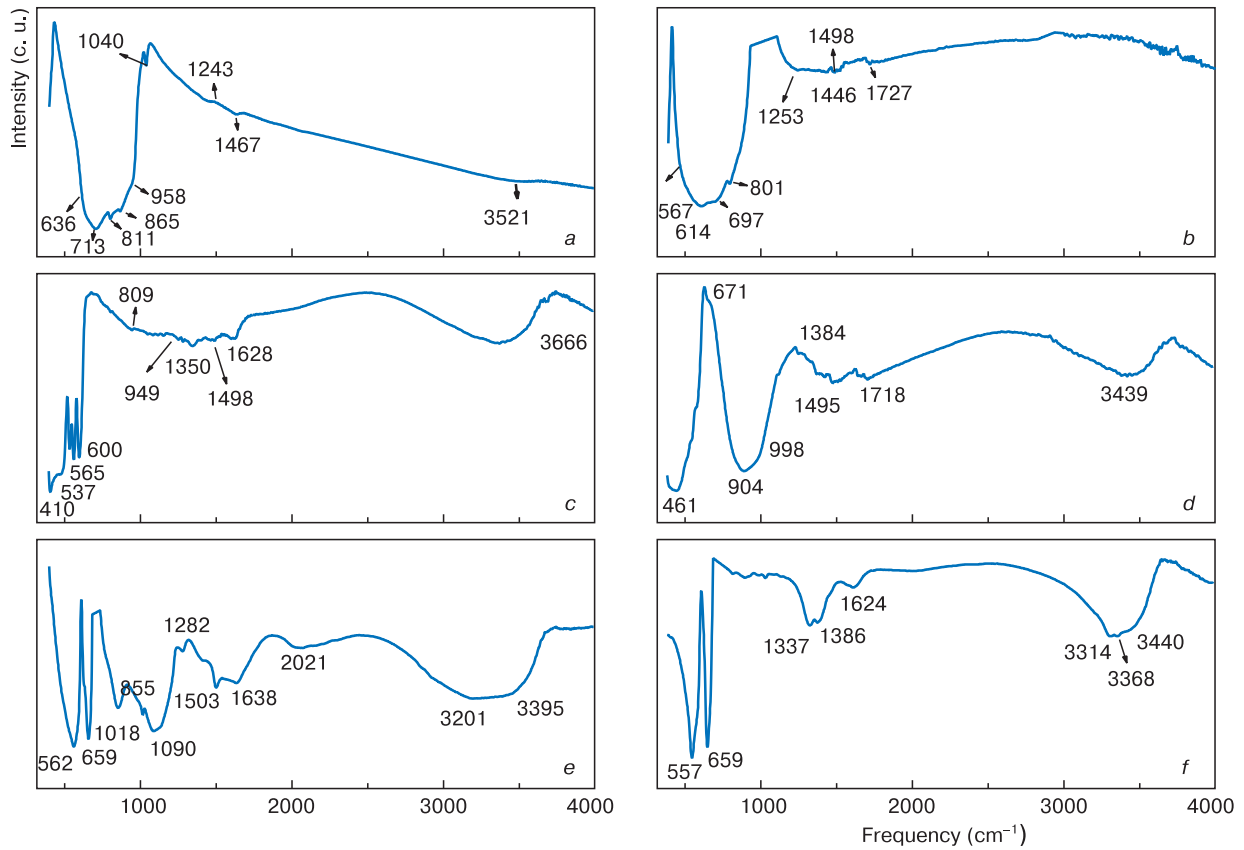


Figure 4. IR spectra of WO_3 , In_2O_3 , Co_3O_4 and their compositions: (a) WO_3 , annealing at 600 °C (2 h), (b) WO_3 , annealing at 600 °C (2 h), after exposure to a gas-air mixture containing 3.6 ppm NO_2 ($T = 187$ °C, $t = 30$ min.), (c) In_2O_3 , annealing at 600 °C (2 h), (d) In_2O_3 , annealing at 600 °C (2 h), after exposure to a gas-air mixture containing 3.6 ppm NO_2 ($T = 187$ °C, $t = 30$ min.), (e) Co_3O_4 , annealing at 450 °C (2 h), (f) Co_3O_4 , annealing at 600 °C (2 h).

WO_3 [12–15]. The respective bands are present in the spectra of the samples dried at 20 °C (tungstic acid) and 300 °C. The spectrum of the unannealed specimen had an absorption band in the 3100–3550 cm^{-1} region caused by the O–H oscillations (symmetrical and asymmetrical) of coordination bound water. The 1600 cm^{-1} band seems to refer to the HOH bonds in H_2O and the 914.7, 939.9 and 1003.6 cm^{-1} bands are also related to coordination water (the W– OH_2 bond). The WO_3 specimens treated in a gas and air atmosphere containing NO_2 had a different absorption pattern in the 1200–1700 cm^{-1} region. They contained bands at 1253.0, 1446.3 and 1498.4 cm^{-1} which seem to refer to the valence and deformation oscillations of adsorbed NO_2 (there are no available literary data for comparison). Figure 4a shows an IR spectrum of WO_3 annealed at 600 °C for 2 h and Fig. 4b shows an IR spectrum of the same WO_3 specimen heat-treated in a gas and air atmosphere containing 3.6 ppm NO_2 ($T = 187$ °C $t = 30$ min).

Only the $\text{In}(\text{OH})_3$ xerogel spectrum has a strong absorption peak in the 780–1153 cm^{-1} oscillation region corresponding to In–OH bond oscillations whereas heat-treated specimens exhibited little if any absorption in this region. This indicates a low OH group concentration already after heat treatment at 300 °C. Also In–

(OH)₃ exhibits strong absorption in the 1428–1545 cm^{-1} region which is weaker for the specimen annealed at 300 °C and even weaker for the specimen annealed at 600 °C (Fig. 4c). Absorption near 1500 cm^{-1} is caused by In–O oscillations. The absorption bands at 1385 and 1640 cm^{-1} should be attributed to bond oscillations of nitrate ions and deformation oscillations in water, respectively [15–17]. The In_2O_3 specimens treated in a gas and air atmosphere containing 3.6 ppm NO_2 (Fig. 4d) has a wide absorption band in the 900–1000 cm^{-1} region. There are also bands at 904.8 and 998.5 cm^{-1} which seem to refer to valence and deformation oscillations of adsorbed NO_2 .

The Co_3O_4 spectra have peaks at 500–900 cm^{-1} correspondings to Co–O oscillations. Absorption in the 900–2500 cm^{-1} region is associated with Co–OH oscillations. The spectrum is shown in Fig. 4d also has a band in the 3100–3550 cm^{-1} region caused by O–H oscillations (symmetrical and asymmetrical) of coordination bound water. The 1600 cm^{-1} band refers to HOH bonds in H_2O and the bands at 914.7, 939.9 and 1003.6 cm^{-1} are related to oscillations of coordination water. Valence and deformation oscillations of adsorbed NO_2 cause the wide and intense bands in the 800–1100 cm^{-1} region (peaks at 854.6, 1018.3 and 1089.7 cm^{-1} in Fig. 4e [18–20]).

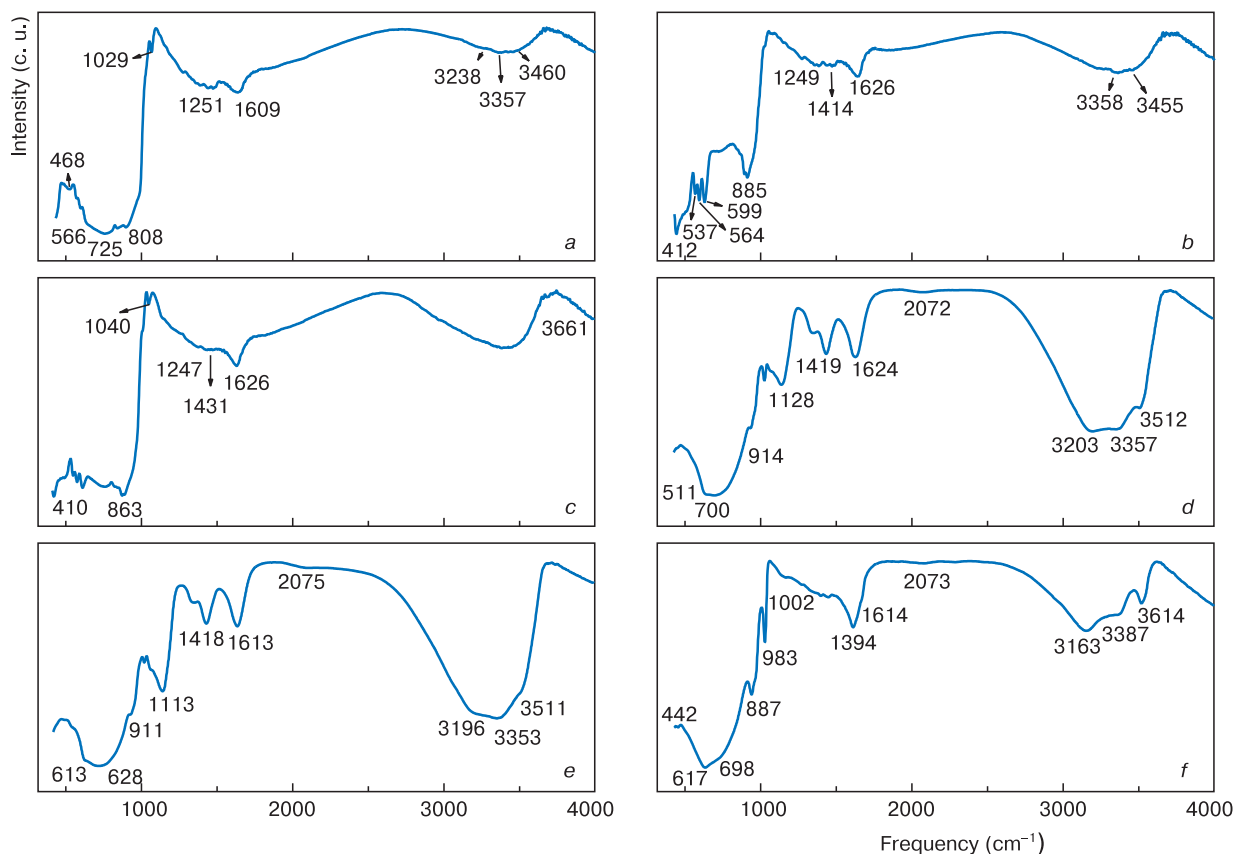


Figure 5. IR spectra of samples of compositions $\text{WO}_3\text{-In}_2\text{O}_3$ and $\text{WO}_3\text{-Co}_3\text{O}_4$: (a) 25InW, (b) 50InW, (c) 75InW, (d) 15CoW, (e) 25CoW, (f) 50CoW.

The cubic structure of Co_3O_4 contains Co^{2+} ($3d^7$) and Co^{3+} ($3d^6$) located in tetrahedral and octahedral sites, respectively, and has the $Fd\bar{3}m$ space symmetry group. The bands at $556.1\text{--}655.7\text{ cm}^{-1}$ are related to valence oscillations of Co–O bonds and are typical of cubic Co_3O_4 , but also could belong to impurities of CoO and Co_3O_4 which are hard to detect with IR spectroscopy [21].

The shapes, intensities and locations of the two narrow bands at 664.69 and 568.74 cm^{-1} correspond to the mono-disperse fcc structure of Co_3O_4 [22].

There are no literary data available on the origin of the absorption band at 826 cm^{-1} . Since this band does not show for the specimen annealed at $600\text{ }^\circ\text{C}$ it can probably be attributed to adsorbed precursor ion decomposition products. For the same reason (high-temperature desorption) the bands in the $1300\text{--}2500\text{ cm}^{-1}$ region can be associated with oscillations of carboxyl and carboxylate forms of C–O bonds in adsorbed carbon oxide.

The spectra of the 25InW, 50InW and 75InW specimens (Fig. 5a–c) do not exhibit strong absorption in the $900\text{--}3700\text{ cm}^{-1}$ region, by analogy with the WO_3 and In_2O_3 specimens annealed under the same conditions. The $900\text{--}3700\text{ cm}^{-1}$ region refers to symmetrical and asymmetrical O–H bond oscillations in coordination bound water, O–H bond oscillations in water molecules, W–OH₂ bond oscillations and other oscillations relating to coordination

bound water. However, absorption in this region becomes more intense with an increase in the In_2O_3 content suggesting the presence of some In–OH bonds even after annealing at $600\text{ }^\circ\text{C}$. This phenomenon is untypical for tungsten oxide, which usually loses all hydroxyl groups.

Absorption in the $450\text{--}900\text{ cm}^{-1}$ region is related to W–O oscillations in WO_3 and H_2WO_4 as well as In–OH and In–O oscillations in $(\text{InOH})_3$ and In_2O_3 . The ν [In–O] oscillations near 410 cm^{-1} that are typical of In_2O_3 observe in the spectra of the 50InW and 75InW specimens but absent in the 25InW.

Bands referring to W–O bond oscillations in the $\text{WO}_3\text{-In}_2\text{O}_3$ composition spectra are slightly shifted to the left. For example, the band at 706.9 cm^{-1} in the WO_3 spectrum is observed at 725.4 cm^{-1} in the 25InW specimen spectrum and 747.7 cm^{-1} in the 75InW spectrum. This fact may point to a small mutual solubility of the oxides, e.g. probability of indium atom incorporation into the WO_3 lattice [23].

Absorption in the $3200\text{--}3700\text{ cm}^{-1}$ region (oscillations of surface OH groups or bonds in adsorbed water molecules) and at 1626 cm^{-1} (deformation water oscillations) in the IR spectrum of WO_3 annealed at $600\text{ }^\circ\text{C}$ is almost absent. However, indium oxide annealed under the same conditions has strong absorption bands in that region. An increase in the In_2O_3 content in the $\text{WO}_3\text{-In}_2\text{O}_3$ composition from 25.0 to 75.0 wt.% leads to an increase in the absorption band intensity in that region. The intensity of

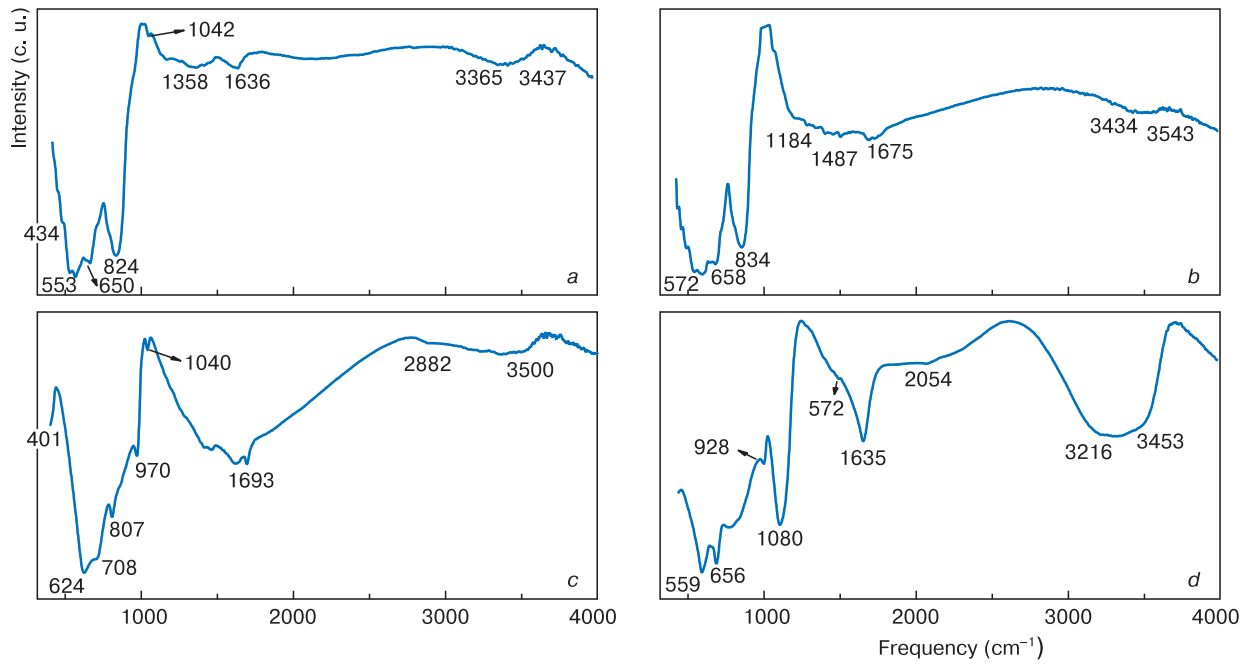


Figure 6. IR spectra of the compound CoWO_4 and samples of the composition $\text{WO}_3\text{-Co}_3\text{O}_4$: (a) CoWO_4 , synthesis 650°C , 2 h, (b) CoWO_4 , synthesis 650°C , 2 h, after exposure to a gas-air mixture containing 3.6 ppm NO_2 ($T = 187^\circ\text{C}$, $t = 30$ min.), (c) 5 wt.% Co_3O_4 , 450°C , 2 h, (d) 15 wt.% Co_3O_4 , 450°C , 2 h.

the absorption bands in the 75InW specimen is the same as for the In_2O_3 specimen. Thus materials with different WO_3 to In_2O_3 content ratios have different surface properties. Analysis of the IR spectra suggests a higher adsorption capacity of the $\text{WO}_3\text{-In}_2\text{O}_3$ composition as compared to that of the source oxides due to the retained high concentration of surface OH groups (close or equal to that of In_2O_3).

Analysis of the IR spectra confirms the conclusions made from the X-ray phase analysis data concerning the formation of CoWO_4 as a result of joint annealing of tungstic acid and cobalt hydroxide sols at $600\text{--}650^\circ\text{C}$ for 2 h. Usually, there are characteristic bands of metal oxides at low-frequency region ($500\text{--}600\text{ cm}^{-1}$) (in our case Co_3O_4 bands band are absent). The absorption bands near 1000 cm^{-1} can be attributed to oscillations of deformed Co–O, W–O and W–O–W bonds. The most clearly seen is the band at 500 cm^{-1} correspondings to W–O bonds in WO_6 octahedra. Moreover, the bands at 821 and 620 cm^{-1} are directly related to valence oscillations of O–W–O and W–O bonds. The bands at 1635 and 3300 cm^{-1} refer to O–H bond oscillations of coordination bound and physically adsorbed water molecules [18–22].

The experimental IR spectra indicate the presence of separated WO_3 and Co_3O_4 phases in the powders. The $\text{WO}_3\text{-Co}_3\text{O}_4$ composition specimen (15.0 wt.%, 15CoW) treated in a gas and air atmosphere containing NO_2 (Fig. 5d) exhibits intense absorption in the $1100\text{--}1700\text{ cm}^{-1}$ region. This may indicate NO_2 adsorption by surfaces of WO_3 and Co_3O_4 particles. Absorption in this region is commonly attributed to different adsorbed forms of nitrogen dioxide. The $1500\text{--}1700\text{ cm}^{-1}$ region has a NO_2

absorption peak and the $2000\text{--}2250\text{ cm}^{-1}$ region has a CO absorption peak [23].

Figure 6a, b show IR spectra of WCoO_4 powder before and after treatment in a gas and air atmosphere containing NO_2 . There is no intense absorption in the frequency region corresponding to the oscillation frequency of adsorbed NO_2 bonds and hence the gas adsorption capacity of CoWO_4 is lower than that of WO_3 and Co_3O_4 two-phase composition.

Figure 6c, d show IR spectra of the 5CoW and 15CoW specimens heat-treated at 400°C for 2 h. The $900\text{--}3700\text{ cm}^{-1}$ region corresponding to symmetrical and asymmetrical oscillations of O–H bonds in coordination bound water molecules, W–OH₂ bond oscillations and other oscillations has more intense absorption than for the WO_3 and Co_3O_4 specimens annealed under the same conditions. This can be caused by slower WO_3 and Co_3O_4 dehydration and crystallization in compositions than in simple oxides. The higher concentration of surface OH groups may favor the higher adsorption capacity of the composition in comparison with the source oxides.

Absorption in the $450\text{--}900\text{ cm}^{-1}$ region is caused by W–O oscillations in WO_3 and H_2WO_4 as well as Co–OH and Co–O oscillations in $\text{Co}(\text{OH})_2$ and Co_3O_4 . There were no new absorption bands related to the possible formation of chemical compounds including CoWO_4 during annealing at 450°C found. This result is in agreement with the X-ray phase analysis data.

The ν [In–O] and ν [Co–O] oscillations at $656\text{--}659$ and $553\text{--}557\text{ cm}^{-1}$ typical of cobalt oxide are present in the 15InW specimen spectrum at 559.3 and 656.0 cm^{-1} . This indicates that there is no shifting typical of Co_3O_4 base solid solution formation. The bands of W=O and W–O

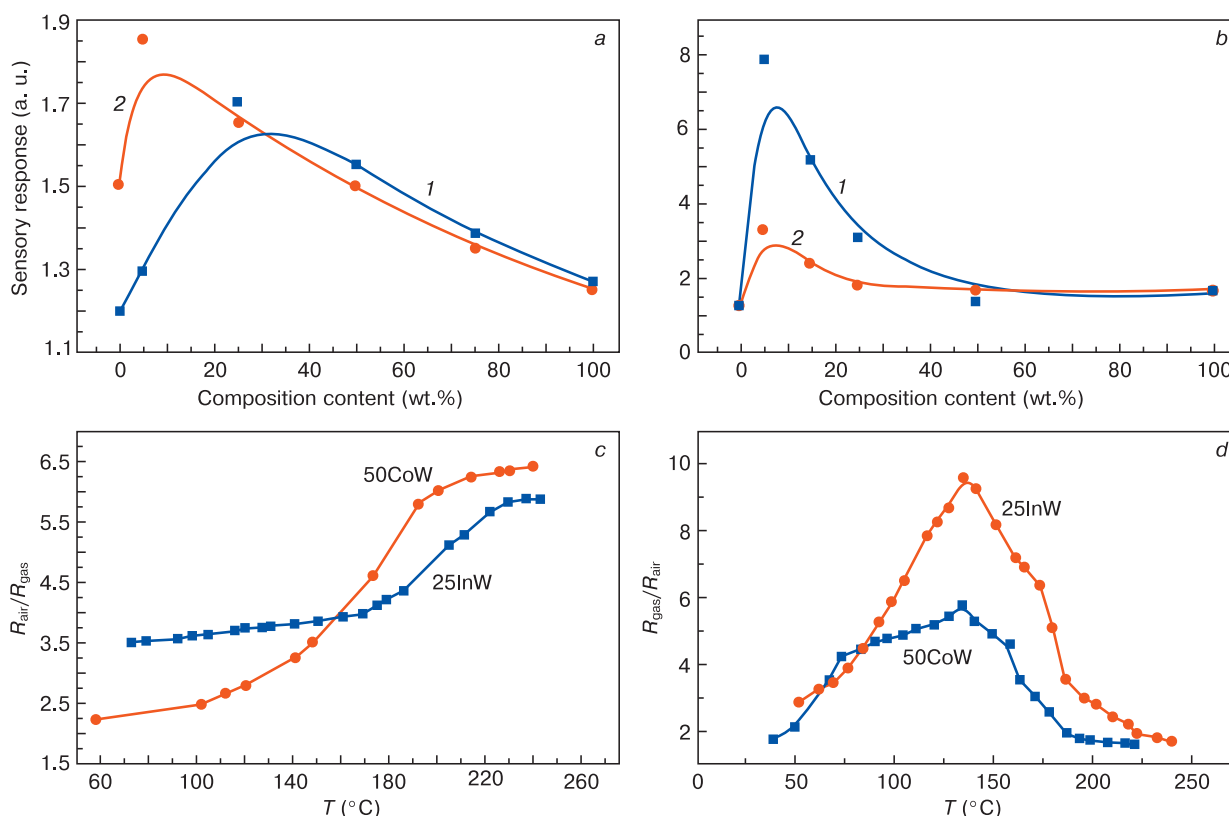


Figure 7. Sensory response of samples of $\text{WO}_3\text{-In}_2\text{O}_3$ compositions (gas-porous tablets) depending on composition (a, b) and temperature (c, d): (a) CO/air, 3000 ppm, 242 °C ((1) $\text{WO}_3\text{-In}_2\text{O}_3$, (2) $\text{WO}_3\text{-Co}_3\text{O}_4$), (b) NO_2 /air, 1.1 ppm ((1) $\text{WO}_3\text{-In}_2\text{O}_3$, (2) $\text{WO}_3\text{-Co}_3\text{O}_4$), (c) 3000 ppm CO/N_2 , (d) 1.1 ppm NO_2 /air. Gas supply time – 10 min.

bond oscillations were at 636.8, 809.3, 967.8 and 1038.9 cm^{-1} in the WO_3 spectrum and at 620.1, 811.3, 972.1 and 1079.7 cm^{-1} in the 15CoW spectrum. This is another indication of the significant dissolution of cobalt oxide in the tungsten oxide structure. Stronger low-frequency shifts are typical of absorption bands for $\nu[\text{W-OH}_2]$ bond oscillations (1038.9, 1409.8, 1452.0 and 1624.2 cm^{-1}), and the higher intensity of these bands, especially the one at 1635 cm^{-1} testifies to a higher concentration of the respective surface bonds (chemisorbed water).

Figure 7 shows sensor response of $\text{WO}_3\text{-In}_2\text{O}_3$ and $\text{WO}_3\text{-Co}_3\text{O}_4$ to several air-based gas mixtures as a function of composition (In_2O_3 or Co_3O_4 contents, Fig. 7a, b) and temperature (ratio of specimen resistivity in a gas atmosphere to specimen resistivity in the air for NO_2 and ratio of specimen resistivity in the air to specimen resistivity in a gas atmosphere for CO, Fig. 7c, d).

The highest sensor response to CO was observed in the 180–240 °C range for the $\text{WO}_3\text{-In}_2\text{O}_3$ composition specimens and in the 190–240 °C range for the $\text{WO}_3\text{-Co}_3\text{O}_4$ composition (Fig. 7a). For NO_2 containing gas and air mixture, the ratio of specimen resistivity in the gas and air atmosphere to that in the air for specimens of both compositions is the highest at 140–150 °C.

The expressed temperature dependence of semiconductor gas sensor response is primarily accounted for by the fact that CO molecules with insufficient thermal ener-

gy enter into reaction with oxygen adsorbed on the sensor surface, this reaction being well-known as follows: $\text{CO} + 1/2\text{O}_2 \rightarrow \text{CO}_2$. An increase in the operating temperature increases the thermal energy of adsorbed CO molecules to a level sufficient for overcoming the activation energy barrier and reaction with adsorbed oxygen.

Furthermore, the conductivity of oxides increases with temperature due to high electron mobility. Further increase in temperature may reduce the sensitivity due to a transformation of adsorbed oxygen particles which will trap more electrons from the sensor material and reduce its gas adsorption capacity.

Gas pore containing tungsten oxide pellets showed a somewhat higher sensitivity to both CO and NO_2 containing gas mixtures than indium oxide specimens. However, the mixed specimens have higher sensitivities.

The 25InW specimen has the highest sensor response but further increase in the content of the addition reduces the sensitivity of the material. Sensor response may increase for several reasons. Along with an increase in the specific surface area of mixed compositions (Table 1) which leads to an increase in the number of adsorbed molecules, it also should be taken into account the more complex defect structure of the two oxides in the mixed composition as confirmed by IR spectroscopy. The formation of defects of different origins may significantly change the type of conductivity due to the greater number of free

or delocalized electrons and hence a higher effective carrier concentration on the surface of sensitive materials.

The response of the 5InW specimen is the highest after exposure to a gas and air mixture containing nitrogen dioxide. Along with the abovementioned factors controlling the CO sensitivity of the material, for NO_2 one should also take into account the presence of highly charged states $\text{W}^{3+}\text{-W}^{5+}$ which presumably exhibit specific adsorption to nitrogen oxides. This may cause a shift of the sensitivity maximum due to a decrease in the number of these centers with an increase in indium oxide content.

Figure 7a also shows that the addition of Co_3O_4 increased the CO sensor response in the entire addition concentration range, with the 5CoW specimen having the highest sensitivity. The tungsten oxide specimens had an *n*-type response to CO containing gas mixtures, the cobalt oxide specimens had a *p*-type response, the mixed 5CoW, 15CoW and 25CoW specimens had an *n*-type response to this gas mixture and the 50CoW specimen had a *p*-type response.

The increase in CO sensitivity is probably caused by the catalytic activity of cobalt oxides during oxidation of CO, H_2 and hydrocarbons [17–19]. Authors of [17] suggested that the exceptionally high sensitivity of the $\text{SnO}_2\text{-Co}_3\text{O}_4$ compositions to CO and hydrogen is caused by a change of the oxidation/reduction state of Co_3O_4 .

Unlike the $\text{WO}_3\text{-In}_2\text{O}_3$ composition, for $\text{WO}_3\text{-Co}_3\text{O}_4$ one should also take into account possible formation of *p-n* heterojunctions which favor dissociation of gas molecules. Partial electron transfer between *p* and *n*-type semiconductors changes the electrical conductivity of the material. In the case considered conductivity electrons transfer from WO_3 grains to Co_3O_4 ones at the $\text{WO}_3/\text{Co}_3\text{O}_4$ heterocontacts thus increasing the electrical resistivity of the composition in air, as was observed in the experiment.

If reducing gases are present in gas and air mixtures (H_2 , CO and hydrocarbons) the decrease in the electrical conductivity of Co_3O_4 is higher than that for WO_3 . Thus conductivity electrons mainly return to the catalytically active oxide Co_3O_4 thus increasing its sensitivity (electron sensibilization) [25]. An increase in the Co_3O_4 additive to > 5 wt.% the sensitivity of the material decreased. This can be accounted for by an increase in the fraction of highly reactive regions that impede gas diffusion in bulk specimens and thin-film sensitive elements.

The sensitizing effect of Co_3O_4 in the $\text{WO}_3\text{-Co}_3\text{O}_4$ composition can be attributed to the activation of gas adsorption reactions which cause Co_3O_4 reduction and *p-n* junction destruction.

The sensor response to NO_2 is the highest for the composition containing 5.0 wt.% Co_3O_4 and with a further increase in its concentration, the sensor response decreases monotonically (Fig. 7b). It can be seen from Fig. 7d the temperature maximum of the NO_2 sensitivity of the composition is at 140 °C and the temperature maximum of the CO sensitivity is at 230 °C.

The reduction of the sensitivities to CO and NO_2 can also be caused by the formation of large amounts of

CoWO_4 ($\text{WO}_3\text{-Co}_3\text{O}_4$ annealing at 600 °C or higher) or $\text{In}_2(\text{WO}_4)_3$ ($\text{WO}_3\text{-In}_2\text{O}_3$ annealing at 800 °C or higher).

The high gas sensitivity of the test oxide compositions allows fabricating two-electrode NO_2 sensors with a low sensitivity threshold (less than 1.0 ppm), with a working temperature of <200 °C and an acceptable response and recovery time [4, 26]. The Minsk Research Institute for Radio Engineering Materials has developed low-power NO_2 sensors with a detection threshold of << 1 ppm for gas and air mixtures [2, 3]. The power consumption of the $\text{WO}_3 + 3$ wt.% In_2O_3 sensors on Si substrates is less than 30 mW at a heating current of 51 mA and that of the $\text{WO}_3 + 5$ wt.% Co_3O_4 sensors on Al_2O_3 substrates is 85 mW at a heating current of 31 mA. An important distinctive feature of the $\text{WO}_3\text{-Co}_3\text{O}_4$ sensors is the noticeably smaller recovery time (10–20 s) in permanent heating mode for 2–11 ppm NO_2 detection in comparison with that of the $\text{WO}_3\text{-In}_2\text{O}_3$ sensors (30–300 s) and tungsten oxide systems known from the literature. For detection of reducing gases the $\text{WO}_3\text{-In}_2\text{O}_3$ sensor recovery time was within 20 s.

4. Conclusion

Experiments showed that stable microstructure can be achieved in nanoheterogeneous $\text{WO}_3\text{-In}_2\text{O}_3$ and $\text{WO}_3\text{-Co}_3\text{O}_4$ compositions. An increase in WO_3 , In_2O_3 , WO_3 and Co_3O_4 grain sizes during heat treatment of mixed compositions is slower than in simple oxides.

Joint annealing of tungsten and indium xerogel powders produced by the sol-gel method leads to the formation of $\text{In}_2(\text{WO}_4)_2$ at 800–850 °C. WCoO_4 forms in the $\text{WO}_3\text{-Co}_3\text{O}_4$ system at 600–650 °C. indium tungstate is not as active as the sensitive element of gas sensors. Indium tungstate localization on the surface or in the superficial layer impedes electron interaction between tungsten oxide and indium oxide and reduces the gas adsorption capacity (CO and NO_2 sensitivity) of the $\text{WO}_3\text{-In}_2\text{O}_3$ oxide composition. The formation of the third CoWO_4 phase impedes electron interaction between tungsten oxide and cobalt oxide and reduces the gas adsorption capacity (CO and NO_2 sensitivity) of the $\text{WO}_3\text{-Co}_3\text{O}_4$ oxide composition.

All the experimental $\text{WO}_3\text{-In}_2\text{O}_3$ compositions containing 3.0–50.0 wt.% In_2O_3 or Co_3O_4 have greater CO and NO_2 sensitivity than the source oxides. The highest NO_2 response was at ~140 °C and the highest CO response, at ~230 °C. Cobalt oxide addition to tungsten oxide more effectively increases the CO response of tungsten oxide, and indium oxide addition more effectively increases the NO_2 response. The increase in the gas sensitivity and the reduction of the working temperature of the sensors based on oxide compositions in comparison with the sensors based on the source oxides can be accounted for by structural disordering during heat treatment of the compositions, reduction of grain sizes, an increase in the specific surface area and, for the $\text{WO}_3\text{-Co}_3\text{O}_4$ composition, the formation of *p-n* junctions.

References

- Barsan N., Koziej D., Weimar U. Metal oxide-based gas sensor research: How to? *Sensors and Actuators B: Chemistry*, 2007; 121: 18–35. <https://doi.org/10.1016/j.snb.2006.09.047>
- Haiduk Y.S., Lomonosov V.A., Savitsky A.A. Physico-chemical properties of oxide composition $\text{WO}_3\text{-In}_2\text{O}_3$ prepared by the sol-gel method. *Vestnik BGU. Ser. 2, Khimiya. Biol. Geogr.*, 2016; (3): 36–44 (In Russ.). <http://elib.bsu.by/handle/123456789/171465>
- Haiduk Yu.S., Lomonosov V.A., Savitsky A.A. Physico-chemical properties of oxide composition $\text{WO}_3\text{-Co}_3\text{O}_4$, prepared by the sol-gel method. *Izvestiya Natsional'noi Akademii nauk Belarusi. Seriya khimicheskikh nauk*, 2015; (2): 9–13. (In Russ.). <https://vestichem.belnauka.by/jour/article/viewFile/148/148>
- Haiduk Y.S., Savitsky A.A., Reutskaya O.G., Taratyn A.A. Semiconductor gas sensors based on the composition of tungsten oxide and indium oxide. *Nano- i mikrosistemnaya tekhnika*, 2018; (4): 232–242. <https://doi.org/10.17587/nmst.20.232-242> (In Russ.)
- Haiduk Yu.S., Khort A.A., Lapchuk N.M., Savitsky A.A. Study of $\text{WO}_3\text{-In}_2\text{O}_3$ nanocomposites for highly sensitive CO and NO_2 gas sensors. *J. Solid State Chemistry*, 2019; 273: 25–31. <https://doi.org/10.1016/j.jssc.2019.02.023>
- Iveronova V.I., Revkievich G.P. Theory of X-ray scattering. Moscow: Izdatelstvo Mkovskogo universiteta, 1978, 278 p. (pp. 136–139). (In Russ.)
- Klyachko-Gurvich A.L. A simplified method for determining the surface by air adsorption. *Izvestiya Akademii Nauk SSSR. Seriya khimicheskikh nauk*, 1961; (10): 1884–1886. (In Russ.)
- Krichmar S.I., Bezpál'chenko V.M., Mishekin A.A. A simple method for obtaining calibration gas mixtures. *Zavodskaya laboratoriya. Diagnostika materialov*, 2008; 74(1): 21–22. (In Russ.)
- Kang S.-J.L. Sintering: densification, grain growth and microstructure. Butterworth-Heinemann, 2005, 279 p.
- Kumar V.Bh., Mochanta D. Formation of nanoscale tungsten oxide structures and colouration characteristics. *Bulletin of Material Science*, 2011; 34(3): 435–442. <https://doi.org/10.1007/s12034-011-0117-1>
- Noguera H., Cavaliero A., Rocha J., Trindade T., Pedrosa J.J. Synthesis and characterization of tungsten trioxide powders prepared from tungstic acids. *Materials Research Bulletin*, 2004; 39: 683–693. <https://doi.org/10.1016/j.materresbull.2003.11.004>
- Shi J., Hu G., Cong R., Bu H., Dai N. Controllable synthesis of $\text{WO}_3 \times n\text{H}_2\text{O}$ microcrystals with various morphologies by a facile inorganic route and their photocatalytic activities. *New J. Chemistry*, 2013; 37(5): 1538–1544. <https://doi.org/10.1039/c3nj41159a>
- Ștefan M., Bica E., Muresan L., Grecu R., Indrea E., Trif M., Popovici E. J. Synthesis and characterisation of tungsten trioxide powder prepared by sol-gel route. *J. Optoelectronics and Advanced Materials*, 2010; 2(1): 115–118.
- Nogueira H., Cavaleiro A., Rocha J., Trindado T., Pedrosa de Jesus J. Synthesis and characterization of tungsten trioxide powders prepared from tungstic acids. *Materials Research Bulletin*, 2004; 39: 683–693. <https://doi.org/10.1016/j.materresbull.2003.11.004>
- Shimizu Y., Matsunaga N., Hyodo T., Egashira M. Improvement of SO_2 sensing properties of WO_3 by noble metal loading. *Sensors and Actuators B: Chemical*, 2001; 77: 35–45. [https://doi.org/10.1016/S0925-4005\(01\)00669-4](https://doi.org/10.1016/S0925-4005(01)00669-4)
- Sobotta H., Neumann H., Küchn G., Riede V. Infrared lattice vibrations of In_2O_3 . *Crystal Research and Technology*, 1990; 25(1): 61–64. <https://doi.org/10.1002/crat.2170250112>
- Liu G. Synthesis, characterization of In_2O_3 nanocrystals and their photoluminescence property. *Int. J. Electrochem. Sci.*, 2011; 6(6): 2162–2170. <http://www.electrochemsci.org/papers/vol6/6062162.pdf>
- Salavati-Niasari M., Mir N., Davar F. Synthesis and characterization of Co_3O_4 nanorods by thermal decomposition of cobalt oxalate. *J. Phys. Chem. Solids*, 2009; 70(5): 847–852. <https://doi.org/10.1016/j.ica.2009.07.023>
- Sharifi S.L., Shakur H.R., Mirzaei A., Hosseini M.H. Characterization of cobalt oxide Co_3O_4 nanoparticles prepared by various methods: effect of calcination temperatures on size, dimension and catalytic decomposition of hydrogen peroxide. *Int. J. Nanosci. Nanotechnol.*, 2013; 9(1): 51–58. http://www.ijnonline.net/article_3880_cf0693bb7ba98dbdd64b6cb4ae3c88de.pdf
- Wöllenstein J., Burgmair M., Plescher G., Sulima T., Hildenbrand J., Böttner H., Eisele I. Cobalt oxide based gas sensor on silicon substrate for operation at low temperatures. *Sens. Actuators B: Chem.*, 2003; 93(1–3): 442–447. [https://doi.org/10.1016/S0925-4005\(03\)00168-0](https://doi.org/10.1016/S0925-4005(03)00168-0)
- Devadatha D., Raveendran R. Structural and dielectric characterization of nickel-cobalt oxide nanocomposite. *J. Material Sci. Eng.*, 2013; S11: 003. <https://doi.org/10.4172/2169-0022.S11-003>
- Tang Ch.-W., Wang Ch.-B., Chien Sh.-H. Characterization of cobalt oxides studied by FT-IR, Raman, TPR and TG-MS. *Thermochimica Acta*, 2008; 473(1–2): 68–73. <https://doi.org/10.1016/j.tca.2008.04.015>
- Khatko V., Llobet E., Vilanova X., Brezmes J., Hubalek J., Malysz K., Corrieg X. Gas sensing properties of nanoparticle indium-doped WO_3 thick films. *Sens. Actuators B: Chem.*, 2005; 111–112: 45–51. <https://doi.org/10.1016/j.snb.2005.06.060>
- Pierson R.H., Fletcher A.N., Clair Gantz E.St. Catalog of infrared spectra for qualitative analysis of gases. *Analytical Chemistry*, 1956; 28(8): 1218–1239. <https://doi.org/10.1021/ac60116a002>
- Choi J.-S., Sakai Go, Shimano K., Yamazoe N. Sensing properties of $\text{SnO}_2\text{-Co}_3\text{O}_4$ composites to CO and H_2 . *Sens. Actuators B: Chem.*, 2004; 98: 166–173. <https://doi.org/10.1016/j.snb.2003.09.033>
- Haiduk Yu.S., Taratyn I.A. Nitrogen dioxide sensor. Application for the invention of the Republic of Belarus. MIIK G01N 27/407; No. a 20140371; appl. 08.07.2014; publ. 28.02.2016. *Aficyjny biulietėń Nacyjanal'naha centra inteliectual'naj ulasnasci Respubliki Bielaruś*, 2016; (1): 44. (In Russ.)